High temperature transport properties of thermoelectric $CaMnO_{3-\delta}$ — Indication of strongly interacting small polarons

M. Schrade, , R. Kabir, , S. Li, , T. Norby, and , and T. G. Finstad

Citation: Journal of Applied Physics **115**, 103705 (2014); doi: 10.1063/1.4868321
View online: http://dx.doi.org/10.1063/1.4868321
View Table of Contents: http://aip.scitation.org/toc/jap/115/10
Published by the American Institute of Physics

Articles you may be interested in

Influence of tungsten substitution and oxygen deficiency on the thermoelectric properties of $CaMnO_{3-\delta}$
Journal of Applied Physics **114**, 243707 (2013); 10.1063/1.4854475

High temperature thermoelectric characteristics of $Ca_{0.9}R_{0.1}MnO_3$ $(R = La, Pr, \ldots, Yb)$
Journal of Applied Physics **104**, 093703 (2008); 10.1063/1.3003065

Thermoelectrical properties of A-site substituted $Ca_{1-x}Re_xMnO_3$ system
Journal of Applied Physics **100**, 084911 (2006); 10.1063/1.2362922

Versatile apparatus for thermoelectric characterization of oxides at high temperatures
Review of Scientific Instruments **85**, 103906 (2014); 10.1063/1.4897489

High-temperature thermoelectric properties of $(Zn_{1-x}Al_x)O$
Journal of Applied Physics **79**, 1816 (1998); 10.1063/1.360976

High-temperature thermoelectric properties of $Ca_{0.9-x}Sr_xYb_{0.1}MnO_{3-\delta}$ $(0 \le x \le 0.2)$
Journal of Applied Physics **105**, 093717 (2009); 10.1063/1.3125450

High temperature transport properties of thermoelectric $CaMnO_{3-\delta}$ — Indication of strongly interacting small polarons

M. Schrade,[1,a)] R. Kabir,[2] S. Li,[2] T. Norby,[3] and T. G. Finstad[1]
[1]*Centre for Materials Science and Nanotechnology, Department of Physics, University of Oslo, Sem Sælandsvei 24, 0371 Oslo, Norway*
[2]*School of Materials Science and Engineering, University of New South Wales, Sydney, New South Wales 2052, Australia*
[3]*Centre for Materials Science and Nanotechnology, Department of Chemistry, University of Oslo, FERMiO, Gaustadalléen 21, 0349 Oslo, Norway*

(Received 31 January 2014; accepted 1 March 2014; published online 13 March 2014)

The conductivity and Seebeck coefficient of $CaMnO_{3-\delta}$ have been studied at temperatures up to 1000 °C and in atmospheres with controlled oxygen partial pressure. Both transport coefficients were varied *in situ* by the reversible formation of oxygen vacancies up to $\delta = 0.15$. The charge carrier concentration was calculated using a defect chemical model. The Seebeck coefficient could be approximated by Heikes' formula, while the conductivity shows a maximum at a molar charge carrier concentration of 0.25. These results were interpreted as a signature of strong electronic correlation effects, and it was concluded that charge transport in $CaMnO_{3-\delta}$ occurs via strongly interacting small polarons. General prospects for strongly correlated materials as potential candidates for high temperature thermoelectric power generation were discussed. © *2014 AIP Publishing LLC*. [http://dx.doi.org/10.1063/1.4868321]

I. INTRODUCTION

Mixed-valent manganites with perovskite-related structures exhibit a rich variety of interesting electrical, structural, and magnetic properties and led to the development of new physical concepts like the superexchange mechanism and to new applications due to their pronounced magnetoresistive effect (see Ref. 1 for a review). Characteristic for these materials is a strong electron-phonon coupling, often leading to a self-localisation of charge carriers by lattice distortions. If the dimension of the carrier and its surrounding lattice distortion is in the range of the interatomic distance, it is named a small polaron and charge transport occurs via thermally activated hopping.[2]

Recently, manganites are also investigated as potential thermoelectric materials. Several classes of 3*d* transition-metal oxides such as layered cobaltites, titanates, or transparent conducting oxides are investigated as candidates for thermoelectric energy harvesting at high temperatures,[3–5] but despite considerable scientific activity within the field, the reported values for the thermoelectric figure of merit zT are still well below other state-of-the-art thermoelectric materials based on more scarce and/or environmentally harmful p-block elements. The highest zT-figures among oxides are reported for layered cobaltites as p-type conducting materials, while zT for n-type oxides is significantly lower (e.g., Ref. 6). Among these n-type thermoelectric oxides, electron doped $CaMnO_{3-\delta}$ is one of the most prominent n-type thermoelectric oxides with a reported maximum $zT = 0.3$ for $CaMn_{0.98}Nb_{0.02}O_3$,[7] making it a typical choice when designing an all-oxide thermoelectric generator.[8,9]

Although it is well established that the oxygen content in $CaMnO_{3-\delta}$ can be varied over a broad range making it an interesting material as a cathode in solid oxide fuel cells[10] or as an oxygen storage material in advanced combustion processes,[11] most of the published high temperature thermoelectric data are taken under atmospheric conditions with the oxygen content of the sample being poorly defined. Therefore, experimental data on nominally identical samples scatter significantly and show opposite temperature trends, and a profound assessment of these materials in thermoelectric applications is not yet possible (e.g., Refs. 12 and 13). Even when measuring in air, oxygen vacancies will form in $CaMnO_{3-\delta}$ and lead to a significant variation on thermoelectric properties at high temperatures.[14]

The defect chemistry of oxygen-deficient $CaMnO_{3-\delta}$ was recently studied by Goldyreva *et al.*[15] and will be summarized here. On the basis of thermogravimetric (TG) measurements, it was found that the defect properties of $CaMnO_{3-\delta}$ can be described by two chemical reactions: (a) The filling of oxygen vacancies accompanied by a oxidation of Mn-sites and (b) the thermal excitation of electronic charge carriers across the band-gap. In the Kröger-Vink-notation,[16] these reactions read

$$\frac{1}{2}O_2(g) + v_O^{\bullet\bullet} + 2Mn'_{Mn} = O_O^x + 2Mn^x_{Mn}, \quad (1)$$

$$2Mn^x_{Mn} = Mn'_{Mn} + Mn^{\bullet}_{Mn}. \quad (2)$$

Thermogravimetric data can be fitted with respect to the equilibrium coefficients for the reactions (1) and (2), K_{Ox} and K_D, respectively. Both reactions show an Arrhenius-type behaviour, where the oxidation reaction (Eq. (1)) is exothermic, while the charge disproportionation (Eq. (2)) is endothermic. The reaction enthalpies depend on the structural state of $CaMnO_{3-\delta}$.[15]

a)Electronic mail: matthias.schrade@smn.uio.no

 © 2014 AIP Publishing LLC

In this paper, we report on our simultaneous measurements of Seebeck-coefficent and electrical conductivity of nominally undoped $CaMnO_{3-\delta}$ at high temperatures and in equilibrium with a well-defined atmosphere. Based on the previously published defect chemical model, we can calculate the concentration of all considered electronic species for the specific temperature and atmospheric composition, in particular the concentration of Mn^{3+}, which we identify with the molar charge carrier concentration x. We will further show that the strong correlation of small polaron charge carriers can lead to a simultaneous decrease in conductivity and Seebeck coefficient and discuss the general perspective for manganites with respect to thermoelectric application.

II. EXPERIMENTAL

Polycrystalline samples were synthesized via standard solid state reaction. Powders of $CaCO_3$ (≥99.0%, Sigma-Aldrich) and MnO_2 (≥99.0%, Sigma-Aldrich) were dried for 2 h at 150 °C and weighed in stoichiometric amounts. The mixed powders were ball milled and calcinated twice at 1000 °C for 24 h, with an intermediate grinding. The obtained powders were pressed into pellets at 100 MPa and sintered in air at 1300 °C for 24 h. Room-temperature X-ray diffraction data were collected using a Philips PANalytical X'pert MPD diffractometer using CuKα-radiation and a step-width of 0.02. All observed peaks could be indexed in agreement with literature[17] and no secondary phase could be detected (Fig. 1(a)). The lattice parameters were determined to $a = 5.30$ Å, $b = 7.47$ Å, and $c = 5.28$ Å (SG *Pnma* (No. 62)). A bar-shaped sample of ca. $3 \times 3 \times 14$ mm^3 in dimension cut from the pellet was mounted into a commercially available measurement cell (ProboStat, NorECs, Norway), which was modified for our purposes (Fig. 1(b)): The sample was clamped into a spring-load system with an S-type thermocouple (PtRh10, Pt) attached on each side in good thermal and electrical contact with the sample. The Pt-leads of each thermocouple were used to measure the thermoelectric voltage across the sample. Two platinum electrodes were tightly wrapped around the sample serving as voltage probes during resistivity measurements. The cell was placed in a vertical tube furnace providing the base temperature of the measurement. The temperature difference across the two sample ends was stepwise varied using a resistive micro-heater placed underneath the sample. The measured thermoelectric voltage was corrected for Pt-lead contribution. The conductivity was measured in four point geometry, using the Pt-wires of the thermocouples as current leads and the two electrodes as voltage probes. The effects of Peltier heating and thermal offsets were taken care of by switching current direction. The oxygen partial pressure in the cell was controlled by diluting O_2 with Ar in a commercial gas mixer (ProGasMix, NorECs, Norway). The relaxation towards chemical equilibrium was monitored measuring the voltage across the two electrodes as a function of time when sending a constant current through the sample. All measurements presented here were taken at thermal and chemical equilibrium, unless otherwise noted.

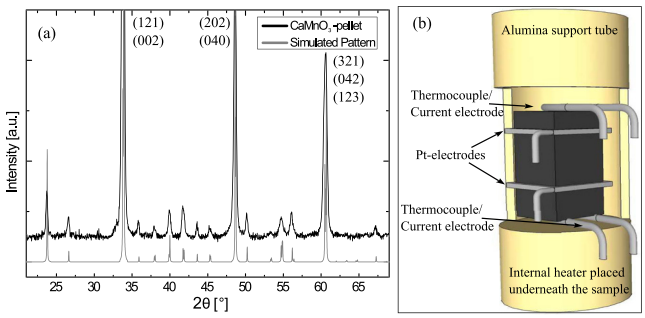

FIG. 1. (a) X-ray diffractogram of the as prepared sample. For comparison, we show a simulated pattern using the extracted lattice parameters and the structural model by Poeppelmeier *et al.*[17] All observed peaks could be indexed and no secondary phase could be detected. (b) The bar-shaped sample mounted into the measurement cell.

III. RESULTS AND DISCUSSION

Since the degree of oxygen non-stoichiometry is reported to vary only slightly over a large range of oxygen partial pressure at lower temperatures,[15] which agrees with our preliminary findings, we restrict our study to temperatures above 800 °C. The equilibrium oxygen nonstoichiometry, the electrical conductivity σ, and the Seebeck coefficient α as a function of temperature and oxygen partial pressure pO_2 are shown in Fig. 2. The negative sign of the thermopower indicates that electrons (here assumed to be localised as Mn^{3+}) are the dominating charge carrier in $CaMnO_{3-\delta}$. The values of σ and α at the highest oxygen partial pressure are in good agreement with literature data (e.g., Refs. 14, and 18–20). The influence of the extrinsic doping decreases when the concentration of oxygen vacancies increases. Therefore, the highest conductivity in Fig. 2(b) of 60 S cm^{-1} is almost identical with values found by Bocher *et al.* on a series of Nb-doped samples $CaMn_{1-x}Nb_xO_3$ with $0.02 < x < 0.08$.[14] The highest power factor $\alpha^2 \times \sigma$ was determined to 1.8 μW K^{-2} cm^{-1} at 900 °C and for an oxygen partial pressure of 1 atm. At higher temperatures and lower pO_2, the unusual doping dependence of the conductivity, discussed in this paper, leads to a significant reduction of the powerfactor (e.g., ≈1.0 μW K^{-2} cm^{-1} at 900 °C and pO_2 of 10^{-3} atm).

A. Influence of a structural phase transition on σ and α

Let us first consider the measurement taken at 800 °C. It is known, that $CaMnO_{3-\delta}$ undergoes a phase change from orthorhombic to tetragonal and finally to cubic when varying the oxygen partial pressure in the range used in the current experiment.[21] The region of existence of the tetragonal phase extends only over a narrow range in pO_2, so that no reliable defect chemical modelling is possible within this phase.

The conductivity and Seebeck coefficient vary linearly with $\log pO_2$ to an oxygen partial pressure of 0.01 atm, where the slope increases. To gain further insight on the influence of this sequence of phase transitions on the transport coefficients, we calculate the charge carrier concentration x as a function of the experimentally chosen pO_2 values via the defect chemical model presented in the introduction (Eqs. (1) and (2)) and by using the thermodynamic parameter K_D reported by Goldyreva *et al.*[15]

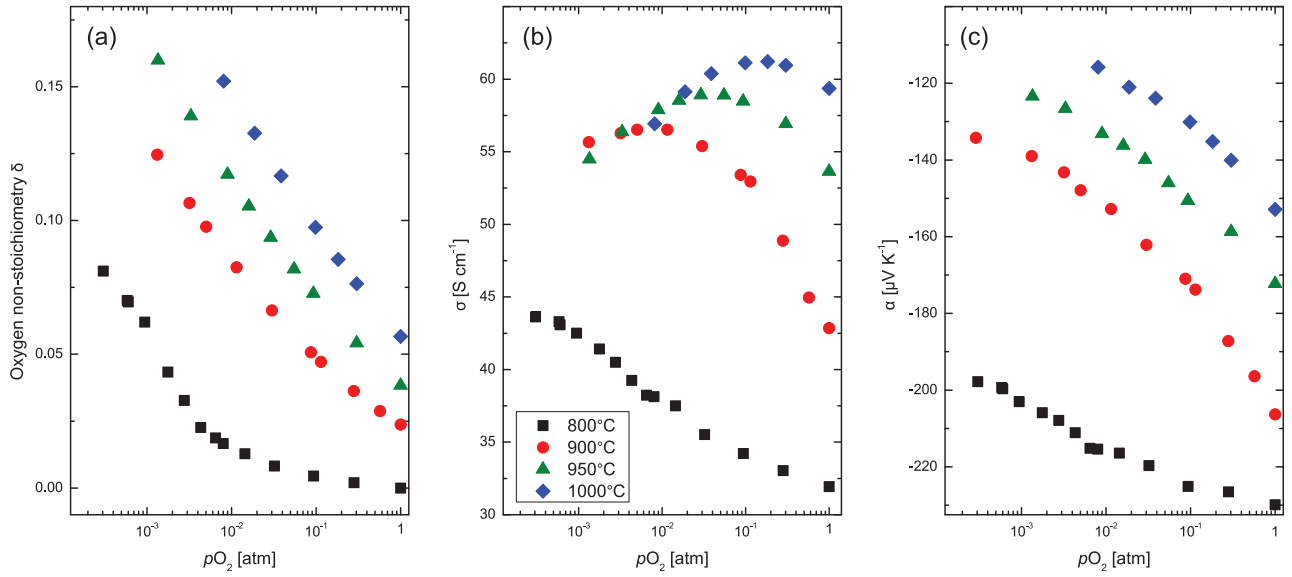

FIG. 2. (a) The oxygen nonstoichiometry δ, (b) the electrical conductivity σ, and (c) the Seebeck coefficient α of $CaMnO_{3-\delta}$ at different temperatures and oxygen partial pressures pO_2.

$$x = 2\delta + \frac{\delta + 2K_D - 4\delta K_D - \sqrt{K_D - 4\delta^2 K_D + \delta^2}}{4K_D - 1}, \quad (3)$$

where x is given as the site fraction of Mn^{3+} per formula unit of $CaMnO_{3-\delta}$. In Fig. 3, we plot the Seebeck coefficient α and the electron mobility μ, calculated by the standard expression

$$\sigma = x\mu Ze, \quad (4)$$

with $Z \times e$ being the charge of each carrier. The Seebeck coefficient α changes steeply with charge carrier concentration in the orthorhombic phase and flattens out in the cubic phase. A widely used high temperature limit for the Seebeck coefficient in localized hopping conductors is the Heikes formula[22,23]

$$\alpha = -\frac{k_B}{e} \times \ln\left[\frac{g_3}{g_4} \times \frac{1-x}{x}\right]. \quad (5)$$

The $g_i = g_{Spin} \times g_{Orbital}$ are the spin and orbital degeneracies of a Mn^{i+}-site. In the cubic phase, the two e_g- and the three t_{2g}-orbitals are degenerate, while in the orthorhombic phase, this degeneracy is lifted. Due to the strong Hund's coupling of Mn-d-electrons, we only consider high-spin configurations here. In the orthorhombic crystal field, the respective factors in Eq. (5) are $g_3 = g_{Sp} \times g_{Or} = 5 \times 1 = 5$ and $g_4 = g_{Sp} \times g_{Or} = 4 \times 1 = 4$, while in the cubic phase, both e_g-orbitals can be occupied and $g_3 = g_{Sp} \times g_{Or} = 5 \times 2 = 10$, while $g_4 = 4$ remains unchanged. This analysis predicts an increase of $|\alpha|$ by $60\,\mu V/K$ when going from the orthorhombic to the cubic phase, independent of the charge carrier concentration x. However, the discrepancy with our observation of a rather continuous change in α can be explained by an energetic splitting of the e_g-orbitals in the orthorhombic phase in the order of k_BT, making both e_g-orbitals thermally accessible, so that the number of available states and thus g_3 do not change when entering the cubic phase.

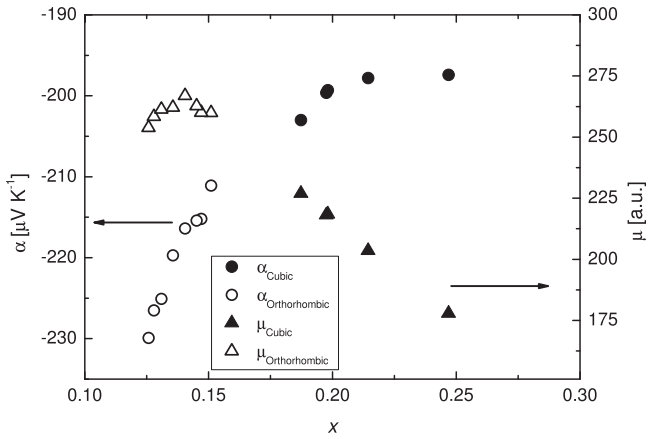

FIG. 3. Mobility μ and Seebeck coefficient α as a function of calculated charge carrier concentration x at 800 °C. No stepwise behaviour can be observed across the phase transition in any of the plots.

In addition, also the carrier mobility calculated from the conductivity via Eq. (4), does not show a discontinuous change across the phase transition (Fig. 3). The mobility of (localised) charge carriers is—in general—a sensitive function of the orbital overlap and thus of the bond-angle of neighbouring species. In the cubic phase of $CaMnO_{3-\delta}$, the angle of a Mn-O-Mn-bond is 180°, while it deviates from that in the tetragonal and orthorhombic phase. Our observation of a continuous change can be explained by a gradual relaxation of this angle to 180° when oxygen vacancies are formed, in agreement with a structural study.[14] However, a clear difference is seen in the variation of μ with carrier concentration x: While $\mu(x)$ appears to be almost constant in the orthorhombic phase and the corresponding low carrier concentrations, it shows a linear decrease in the cubic phase and higher x. This strong decrease cannot be explained by changes in the structure of $CaMnO_{3-\delta}$, which should lead to an increased mobility in the cubic phase, but another mechanism has to be considered.

B. Transport properties in the cubic phase

At higher temperatures, $CaMnO_{3-\delta}$ is in the cubic phase for most of the pO_2-range studied and no discontinuous

behaviour of δ is reported in the literature. The absolute value Seebeck coefficient decreases continuously with increasing δ as it is expected for an increasing charge carrier concentration while the conductivity goes through a broad maximum. This is an unusual result as α and σ generally vary diametrally as a function of charge carrier concentration. To investigate this behaviour in more detail, we again plot α, σ, and μ against the carrier concentration calculated from the defect chemical model (Fig. 4). At the highest measured temperatures, the Seebeck coefficient shows only a weak dependency on temperature and Heikes formula should thus be an appropriate model. Indeed, the calculated curve by Eq. (5) reproduces the magnitude and change of the experimental data to a certain degree, as seen in Fig. 4(c).

If one includes the hitherto neglected population of Mn^{5+} as a possible site for an electron to hop to with a degeneracy $g_5 = g_{Orbital} \times g_{Spin} = 3 \times 3 = 9$, one can calculate the Seebeck coefficient by the weighted average of the two contributions[24]

$$\alpha = -\frac{k_B}{e}\left[\frac{[Mn^{5+}]}{[Mn^{5+}]+[Mn^{4+}]} \times \ln\left(\frac{10}{9}\times\frac{1-x}{x}\right) + \frac{[Mn^{4+}]}{[Mn^{5+}]+[Mn^{4+}]} \times \ln\left(\frac{10}{4}\times\frac{1-x}{x}\right)\right]. \quad (6)$$

The result slightly improves the agreement between calculation and experiment as indicated by the dashed line (calculated for 1000 °C in Fig. 4(c)).

The occurrence of a maximum in conductivity at around $x = 0.24$, which is via Eq. (4) equivalent to a strong decrease of the mobility μ with x (Fig. 4(b)) is more puzzling. It has been observed previously that the conductivity of $CaMnO_{3-\delta}$ at room temperature varies nonmonotoneously with increasing δ.[25] Those authors attribute this behaviour to an ordering of oxygen vacancies accompanied by an ordering of Mn^{3+} and Mn^{4+} species. In this model, electron transport occurs along these charge-ordered stripes, whose density reaches a maximum at $\delta = 0.16$. However, charge ordering is an unlikely scenario at the high temperatures studied within the present work and the maximum conductivity is observed for a δ-value around 0.08, for which no vacancy ordering has been reported (cf., e.g., Ref. 26). As the employed Heikes formula is derived for the case $U \gg k_B T$, where the high on-site repulsion prevents the double occupancy of one Mn-site by two electrons, we suggest the following qualitative model: With increasing oxygen vacancy concentration δ, the number of charge carriers increases to maintain charge neutrality, but at the same time, the number of available sites get reduced

$$\sigma \propto (1-x) \times x. \quad (7)$$

This model has been employed by several authors previously to describe the doping dependency of small polaron hopping conductors (e.g., Refs. 27 and 28). However, it predicts a maximum in conductivity at $x = 0.5$, while the experimental observations for electrons in $CaMnO_{3-\delta}$ (this study) and holes in $La_{1-x}Ca_xMnO_3$[28] find a maximum around $x = 0.25$. Apparently, the simple model in Eq. (7) provides an intuitive tool to reproduce the unusual doping dependency of transport coefficients in $CaMnO_{3-\delta}$, but a more sophisticated model, including more interaction terms than nearest-neighbour Coulomb repulsion, is needed to fully understand the present observation. Assuming that one electron spreads over two lattice sites may well describe the observed conductivity maximum around $x = 0.25$ within Eq. (7) but fails to reproduce the $\alpha(x)$-curve as calculated by Heikes' formula.

Ciuchi and Fratini have recently derived a cluster model to describe the mobility of small polarons interacting via long-range Coulomb forces.[29] In their theory, the mobility of interacting small polarons can be written as

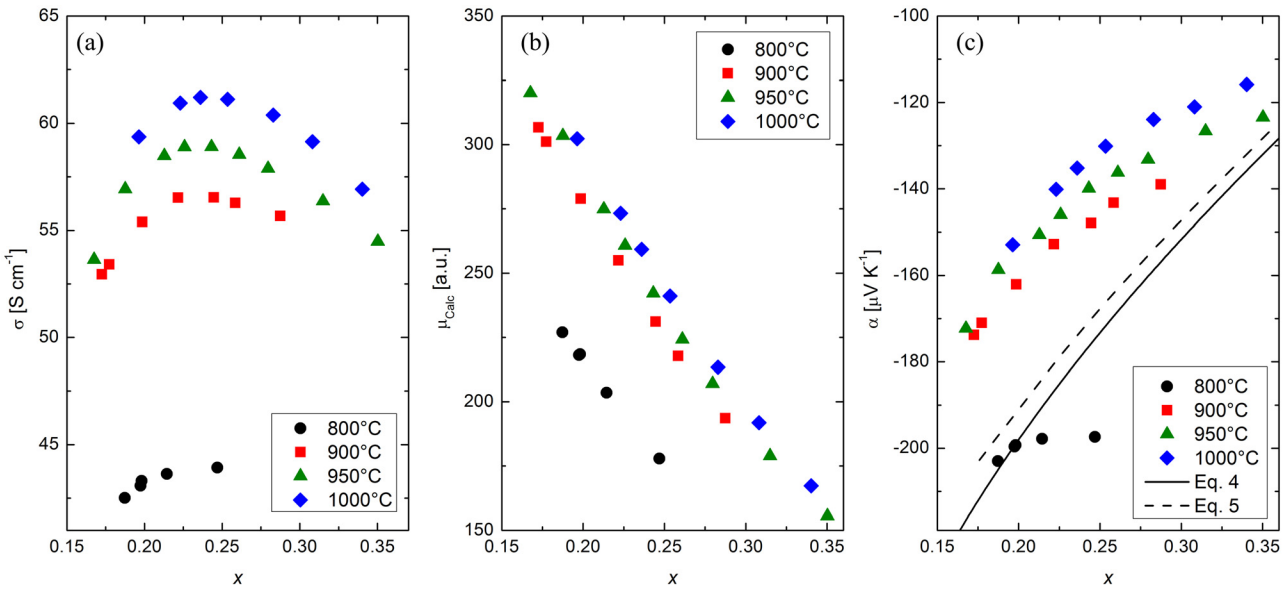

FIG. 4. The electrical conductivity σ (a), the calculated carrier mobility μ (b), and the Seebeck coefficient α (c), in the cubic phase of $CaMnO_{3-\delta}$ as a function of carrier concentration x. σ shows a maximum for $x \approx 0.25$ (a), implying a strong decrease of μ with increasing x via Eq. (4) (b). α can be roughly described by Heikes' formula (c).

$$\mu = \frac{A}{T} \times \exp\left(-\frac{E_a}{k_B T}\right) \times \exp\left(-\frac{E_\xi \times x}{k_B T}\right). \quad (8)$$

If charge transport takes place in three dimensions, E_ξ is given as

$$E_\xi = \frac{\pi e^2}{3\epsilon_0 \times \epsilon_r} \times a^2. \quad (9)$$

A in Eq. (8) comprises parameters like the number of neighbours, the hopping distance, and the hopping attempt frequency and E_a is the activation energy for an electron to hop. In Eq. (9), a is the distance between two polaron sites and ϵ_r is the dielectric permittivity. The introduction of oxygen vacancies not only changes the concentration of electrons in the system but also decreases the effective number of nearest neighbours (both occupied and unoccupied ones), as hopping is only possible if the orbital overlap within the Mn-O-Mn-bridge is finite. It is therefore reasonable to assume $A = (3-\delta) \times A^*$. An additional factor $(1-x)$ compared to Eq. (8) ensures that the mobility is 0 when all manganese sites are filled ($x = 1$). We rewrite the expression for the mobility

$$\mu^*(x) = \frac{\mu_{Calc}}{3-\delta} = B \times (1-x) \times \exp\left(-\frac{E_\xi \times x}{k_B T}\right), \quad (10)$$

with $B = \frac{A^*}{T} \times \exp(-\frac{E_a}{k_B T})$. One can see that the mutual repulsion of the polarons ($E_\xi \neq 0$) leads to an effective gradual increase of the apparent activation energy with increasing carrier concentration x. Eq. (10) describes our data to a high degree (Fig. 5), and the corresponding fitting parameters are given in Table I. Both parameters B and E_ξ increase with temperature.

The increase of E_ξ (Eq. (9)) is likely to be due to a decrease of the relative permittivity ϵ_r, rather than a significant increase in hopping distance a. ϵ_r (or the electric polarizability) generally decrease at higher temperatures due to an increased thermal motion of the charged species. From the temperature dependence of the parameter B, it is possible to calculate an estimate of the polaron activation energy

TABLE I. Fitting parameters according to Eq. (10).

Temperature (°C)	B (a.u.)	E_ξ (meV)
800	156	241
900	193	249
950	198	257
1000	210	276

without any correlations present (for example, realised in a sample with very low charge carrier concentration). We obtain 0.28 ± 0.02 eV (Fig. 6). The increase of the apparent activation energy for the present carrier concentrations due to the correlation effect is in the range of $E_\xi \times x \approx 60$ meV.

To conclude the preceding paragraph, we state that the conductivity in $CaMnO_{3-\delta}$ within the cubic phase can be described by small polarons with strong mutual Coulomb repulsion. This behaviour is likely to occur similarly in other related calcium manganite samples with donor dopants as the source for electronic charge carriers instead of oxygen vacancies as in this work. The total apparent activation energy agrees well with the value recently reported in a similar study.[30]

Fast cooling or quenching a sample from a high temperature state with well defined oxygen partial pressure provides a means to obtain samples with a constant δ at lower temperatures. A sample which has been repeatedly prepared in such way is expected to vary only in δ and thus in charge carrier concentration, while other parameters like the unintended doping level, the electronic band gap, the hopping activation energy, or the interatomic distance remain approximately the same. A variation in the apparent hopping activation energy for one sample with different δ can thus be attributed to the mutual repulsive interaction of small polarons as discussed above. Therefore, we annealed one sample at high temperature and in atmospheres with different pO_2, quenched it, and measured the transport properties up to 450 °C. Preliminary thermogravimetric experiments have shown that $CaMnO_{3-\delta}$ is kinetically stable towards reoxidation below ≈500 °C. All

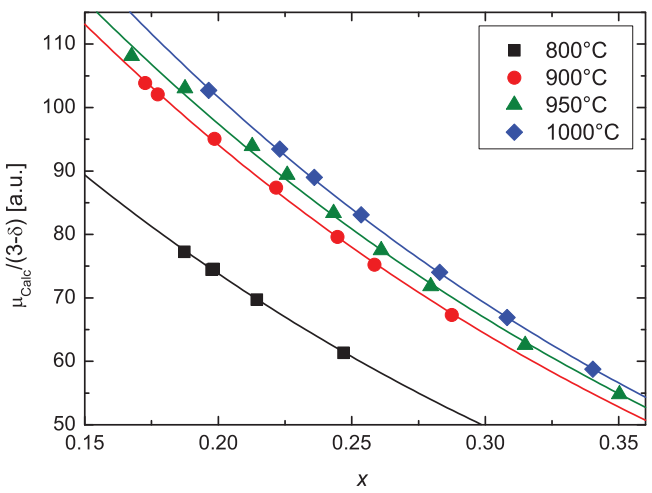

FIG. 5. The normalised mobility in the cubic phase of $CaMnO_{3-\delta}$ vs. calculated carrier concentration. Lines represent the numerical fit via Eq. (10).

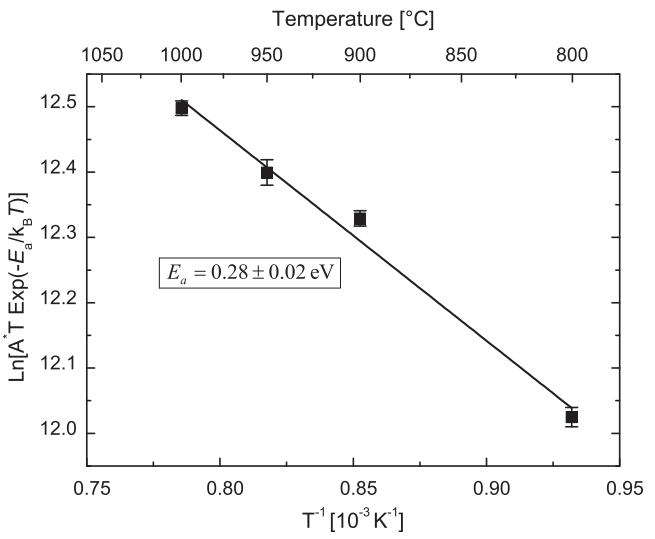

FIG. 6. Arrhenius-type plot of the prefactor B to extract the hopping energy in the absence of electronic correlation.

measurements have been performed on the same sample, quenched from thermodynamic conditions where $CaMnO_{3-\delta}$ is within the cubic phase. As the dense ceramics obtained as described in the Experimental section are prone to develop small cracks due to the thermal stress under quenching, we used a sample sintered at 1100 °C and with a relative density of 75% for this experiment. Reproducibility and internal consistency were confirmed by several repeated heating-quenching cycles. The conductivity decreases with increasing δ and can be described by an activated hopping process for all studied values of δ (Fig. 7). The activation energy increases with increasing δ or charge carrier concentration. In this temperature regime, the carrier concentration is dominated by carriers induced due to oxygen vacancies, and contributions from thermal excitation via Eq. (2) can be neglected. The absolute value of the activation energy around 0.2 eV is less than expected from our high temperature results, where the correlation-free activation energy was determined to be 0.28 eV. On the other hand, the variation in activation energy of 100 meV due to the mutual repulsion of charge carriers is higher than estimated from the high temperature results (via Eq. (10) with $E_\xi \approx 250$ meV and $x = 2 \times \delta$). However, the obtained values agree well with a study of the hole-conductor $La_{1-x}Ca_xMnO_{3-\delta}$.[31] The discrepancy could, for example, be related to an anomaly in resistivity of $CaMnO_{3-\delta}$ around 700 K,[19,32] possibly indicating a different transport mechanism, for example, large polarons, at lower temperatures. In any case, despite an increase in charge carrier concentration by the introduction of oxygen vacancies, the conductivity decreases with δ, indicating a strong interaction of charge carriers.

Finally, we want to discuss shortly the implications of the presented model in the search for new thermoelectric materials. It is instructive to investigate the numerator in zT, the power factor $\alpha^2 \times \sigma$, rather than treating α and σ individually. For the simple model proposed, the power factor can be calculated by combining Eqs. (4), (5), and (10)

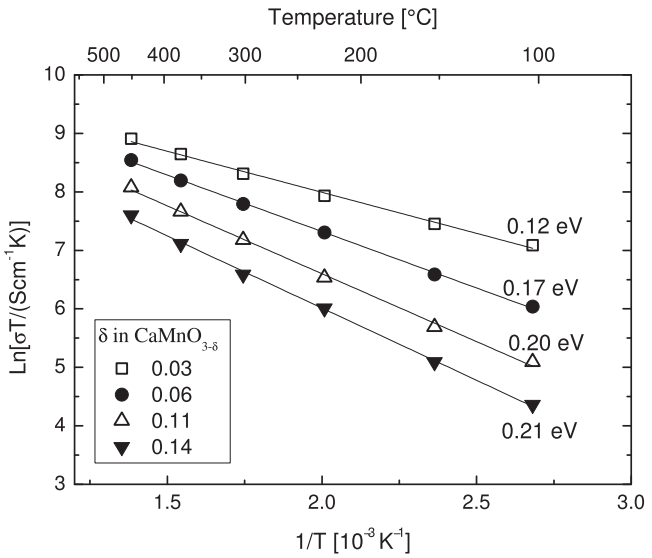

FIG. 7. $\ln \sigma T$ vs. $1/T$ for a sample with different oxygen vacancy concentration. The activation energy increases with increasing δ (or charge carrier concentration).

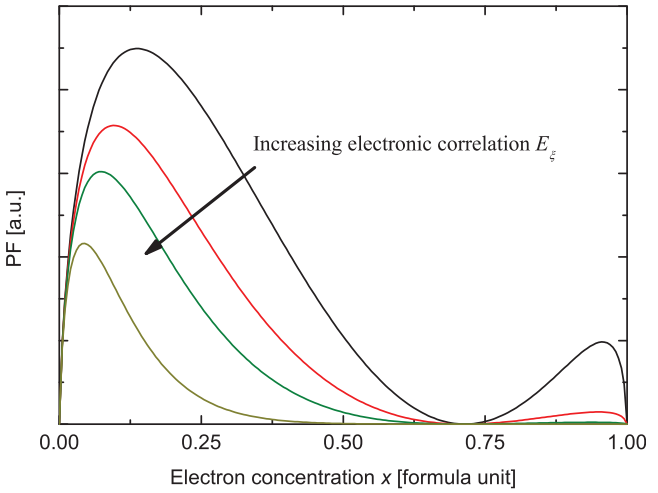

FIG. 8. The power factor $\alpha^2 \times \sigma$ as a function of carrier concentration and for different correlation strengths E_ξ.

$$\alpha(x)^2 \times \sigma(x) \propto \ln\left(\beta \times \frac{1-x}{x}\right)^2 \times \exp(-E_\xi \times x) \times (1-x) \times x, \tag{11}$$

and is schematically shown in Fig. 8. Increasing the strength of mutual Coulomb repulsion via an increase in the parameter E_ξ shifts the maximum of the power factor to lower carrier concentrations or doping levels. Further, does the maximum of the power factor get reduced when other parameters like the bandwidth are kept constant. But the most severe implication of the increased electronic correlation is that the concentration range with $PF(x) \geq PF_{Max}/2$ gets narrower with increasing E_ξ. In materials with a non-constant carrier concentration, e.g., by intrinsic, thermal excitation like in $CaMnO_{3-\delta}$ and its doped compounds, this will lead to a rather sharp peak in zT vs. temperature, thus narrowing the temperature range of optimal performance and finally limit the potential applicability of materials with strong Coulomb repulsion in thermoelectric generators. However, there is experimental evidence for a variable optimal doping concentration (ranging from 0.02 to ≈0.10) for different dopants in $CaMnO_{3-\delta}$, possibly indicating that the strength of correlations depends on the doped species.[7,33]

IV. SUMMARY

In conclusion, we have studied the influence of oxygen non-stoichiometry on the high temperature transport properties of $CaMnO_{3-\delta}$. It is shown that the oxygen stoichiometry in $CaMnO_{3-\delta}$ can be reversibly varied within a broad range up to $\delta = 0.15$ at high temperatures and in different atmospheres allowing significant *in situ* doping of the material. The thermoelectric properties change significantly with varying δ. With increasing δ, an unusual simultaneous decrease of both conductivity and absolute magnitude of Seebeck coefficient is observed. This behaviour can be explained by a conduction process in $CaMnO_{3-\delta}$ at high temperatures via strongly interacting small polarons. The mutual Coulomb repulsion of these polarons quickly reduces the mobility once charge carriers are introduced into the system. The total

activation energy of transport at high temperatures of 0.34 eV was disentangled to consist of two parts: One to be 0.28 eV for $CaMnO_{3-\delta}$ with a negligible carrier concentration and an additional energy $E_{Corr} = E_{\xi} \times x$ due to electronic correlations with E_{ξ} around 0.25 eV and x being the molar charge carrier concentration. The Seebeck coefficient in the studied temperature and carrier concentration range can be described by Heikes' formula to a satisfactorial degree. The present study shows that both thermoelectrical characterisation as well as fundamental analysis of the transport processes in oxides benefit from the careful control of oxygen content.

ACKNOWLEDGMENTS

The authors gratefully acknowledge funding by the Research Council of Norway within the THERMEL Project (143386).

[1]J. M. D. Coey, M. Viret, and S. von Molnár, Adv. Phys. **48**, 167 (1999).
[2]N. Mott and E. Davis, *Electronic Processes in Non-crystalline Materials*, edited by W. Marshall and D. Wilkinson (Clarendon Press, Oxford, 1979).
[3]I. Terasaki, Y. Sasago, and K. Uchinokura, Phys. Rev. B **56**, R12685 (1997).
[4]K. Koumoto, R. Funahashi, E. Guilmeau, Y. Miyazaki, A. Weidenkaff, Y. Wang, and C. Wan, J. Am. Ceram. Soc. **96**, 1 (2013).
[5]S. Hébert and A. Maignan, "Thermoelectric oxides," in *Functional Oxides* (John Wiley & Sons, Ltd, 2010), pp. 203–255.
[6]J. W. Fergus, J. Eur. Ceram. Soc. **32**, 525 (2012).
[7]L. Bocher, M. H. Aguirre, D. Logvinovich, A. Shkabko, R. Robert, M. Trottmann, and A. Weidenkaff, Inorg. Chem. **47**, 8077 (2008).
[8]I. Matsubara, R. Funahashi, T. Takeuchi, S. Sodeoka, T. Shimizu, and K. Ueno, Appl. Phys. Lett. **78**, 3627 (2001).
[9]P. Tomeeš, C. Suter, M. Trottmann, A. Steinfeld, and A. Weidenkaff, J. Mater. Res. **26**, 1975 (2011).
[10]E. Tsipis and V. Kharton, J. Solid State Electrochem. **12**, 1367 (2008).
[11]H. Leion, Y. Larring, E. Bakken, R. Bredesen, T. Mattisson, and A. Lyngfelt, Energy Fuels **23**, 5276 (2009).
[12]J. Park, D. Kwak, S. Yoon, and S. Choi, J. Alloys Compd. **487**, 550 (2009).
[13]C.-J. Liu, A. Bhaskar, and J. J. Yuan, Appl. Phys. Lett. **98**, 214101 (2011).
[14]L. Bocher, M. H. Aguirre, R. Robert, D. Logvinovich, S. Bakardjieva, J. Hejtmanek, and A. Weidenkaff, Acta Mater. **57**, 5667 (2009).
[15]E. Goldyreva, I. Leonidov, M. Patrakeev, and V. Kozhevnikov, J. Solid State Electrochem. **16**, 1187 (2012).
[16]F. Kröger and H. Vink, "Relations between the concentrations of imperfections in crystalline solids," in *Solid State Physics*, edited by F. Seitz and D. Turnbull (Academic Press, 1956), Vol. 3, pp. 307–435.
[17]K. Poeppelmeier, M. Leonowicz, J. Scanlon, J. Longo, and W. Yelon, J. Solid State Chem. **45**, 71 (1982).
[18]Q. He, X. Zhang, H. Hao, and X. Hu, Phys. B **403**, 2867 (2008).
[19]M. Ohtaki, H. Koga, T. Tokunaga, K. Eguchi, and H. Arai, J. Solid State Chem. **120**, 105 (1995).
[20]P. Thiel, J. Eilertsen, S. Populoh, G. Saucke, M. Döbeli, A. Shkabko, L. Sagarna, L. Karvonen, and A. Weidenkaff, J. Appl. Phys. **114**, 243707 (2013).
[21]E. I. Leonidova, I. A. Leonidov, M. V. Patrakeev, and V. L. Kozhevnikov, J. Solid State Electrochem. **15**, 1071 (2011).
[22]P. M. Chaikin and G. Beni, Phys. Rev. B **13**, 647 (1976).
[23]W. Koshibae, K. Tsutsui, and S. Maekawa, Phys. Rev. B **62**, 6869 (2000).
[24]T. D. Sparks, A. Gurlo, and D. R. Clarke, J. Mater. Chem. **22**, 4631 (2012).
[25]J. Briático, B. Alascio, R. Allub, A. Butera, A. Caneiro, M. T. Causa, and M. Tovar, Phys. Rev. B **53**, 14020 (1996).
[26]A. Reller, J. M. Thomas, D. A. Jefferson, and M. K. Uppal, Proc. R. Soc. London, Ser. A **394**, 223 (1984).
[27]S. Mukerjee and J. E. Moore, Appl. Phys. Lett. **90**, 112107 (2007).
[28]D. C. Worledge, L. Miéville, and T. H. Geballe, Phys. Rev. B **57**, 15267 (1998).
[29]S. Ciuchi and S. Fratini, Phys. Rev. B **79**, 035113 (2009).
[30]E. Goldyreva, I. Leonidov, M. Patrakeev, and V. Kozhevnikov, J. Solid State Electrochem. **17**, 1449 (2013).
[31]J. M. De Teresa, K. Dörr, K. H. Müller, L. Schultz, and R. I. Chakalova, Phys. Rev. B **58**, R5928 (1998).
[32]M. E. M. Jorge, M. R. Nunes, R. S. Maria, and D. Sousa, Chem. Mater. **17**, 2069 (2005).
[33]Y. Wang, Y. Sui, H. Fan, X. Wang, Y. Su, W. Su, and X. Liu, Chem. Mater. **21**, 4653 (2009).